

Article

Facile Synthesis and Characterization of Manganese Ferrite Nanoparticles for the Successful Removal of Safranin T Dye from Aqueous Solutions

Zahrah Alhalili ^{1,*} and Ehab A. Abdelrahman ^{2,3,*} ¹ Department of Chemistry, College of Science and Humanities, Shaqra University, Shaqra 11961, Saudi Arabia² Department of Chemistry, College of Science, Imam Mohammad Ibn Saud Islamic University (IMSIU), Riyadh 11623, Saudi Arabia³ Chemistry Department, Faculty of Science, Benha University, Benha 13518, Egypt

* Correspondence: zahalilaili@su.edu.sa (Z.A.); eaaahmed@imamu.edu.sa (E.A.A.)

Abstract: Safranin T dye causes health problems such as skin and respiratory irritations. Hence, the safranin T dye was efficiently removed from aqueous media employing a simply synthesized manganese ferrite (MnFe_2O_4) nanoadsorbent. The synthesis of manganese ferrite nanoparticles was carried out by the pechini sol–gel approach using tartaric acid to serve as a chelating agent in addition to 1,2-propanediol to serve as a crosslinker. The TEM analysis showed that the shape of MnFe_2O_4 nanoparticles is semi-spherical, with an average particle size of 19.32 nm that coincides well with that measured from the XRD (18.89 nm). Further, the several factors that influenced the removal process of safranin T dye were examined, such as time, dye concentration, pH, and temperature. The ideal experimental conditions that achieved the highest safranin T dye removal percentage are pH 8, 80 min, and 298 K. The maximum adsorption capacity of MnFe_2O_4 nanoparticles towards safranin T dye equals 334.45 mg/g. The removal process of safranin T dye by manganese ferrite nanoparticles was chemical, exothermic, and well defined through the Langmuir equilibrium sorption isotherm in addition to the pseudo-second-order model. The synthesized manganese ferrite nanoparticles have the ability to be reused many times without losing their efficiency.

Keywords: MnFe_2O_4 nanoparticles; safranin T dye; adsorption; characterization



Citation: Alhalili, Z.; Abdelrahman, E.A. Facile Synthesis and Characterization of Manganese Ferrite Nanoparticles for the Successful Removal of Safranin T Dye from Aqueous Solutions. *Inorganics* **2024**, *12*, 30. <https://doi.org/10.3390/inorganics12010030>

Academic Editor: Eleonora Aneggi

Received: 1 December 2023

Revised: 5 January 2024

Accepted: 8 January 2024

Published: 15 January 2024



Copyright: © 2024 by the authors. Licensee MDPI, Basel, Switzerland. This article is an open access article distributed under the terms and conditions of the Creative Commons Attribution (CC BY) license (<https://creativecommons.org/licenses/by/4.0/>).

1. Introduction

Dyes and pigments find widespread application in industries such as leather, textile, plastics, printing, pharmaceuticals, rubber, cosmetics, paper, food, and carpet manufacturing to impart color to their products. Annually, over 10,000 distinct dyes, totaling approximately 7×10^5 tons, are manufactured for diverse industrial processes [1–3]. Due to their intricate aromatic structure, many dyes exhibit high resistance to degradation through chemical, physical, and biological treatments. The release of wastewater containing dyes into water bodies presents a significant pollution issue, as these dyes impart undesirable color to the water, diminishing sunlight penetration and reducing gas solubility [4,5]. Safranin T is an organic dye soluble in water, extensively employed in the textile industry. Nevertheless, exposure to Safranin T dye can result in eye burns, potentially causing permanent harm to the cornea and conjunctiva in both human and rabbit eyes. Additionally, contact with Safranin T dye can lead to irritation of the skin and respiratory tract [6]. Hence, it is imperative to treat industrial wastewaters containing such dyes before releasing them into the environment. Various physical and chemical methods, including flocculation [7,8], adsorption [9,10], membrane filtration [11,12], coagulation [13,14], precipitation [15,16], ozonation [17,18], electrochemical techniques [19,20], and fungal decolonization [21,22], have been thoroughly explored for the removal of dyes from aquatic environments. Within these methods, adsorption has demonstrated superiority over other

techniques in eliminating dyes and organic pollutants from process or waste effluents. This superiority is credited to its initial affordability, high effectiveness, uncomplicated design, and operational simplicity. However, a notable drawback of this approach is the elevated cost associated with adsorbents, thereby increasing the overall treatment expenses [23,24]. Using magnetic metal oxides for the removal of heavy metals and dyes offers several advantages such as low cost, ease of synthesis, high adsorption capacity, ease of separation from the treated solution using magnet, and regenerability [25]. Several methods can be employed for preparing magnetic metal oxides such as co-precipitation [26], sol-gel [27], hydrothermal [28,29], spray pyrolysis [30], solid state reaction [31], electrochemical [32], and chemical vapor deposition [33]. The pechini sol-gel method for preparing magnetic metal oxides offers several advantages, such as low crystal size, tailored morphology, low cost, scalability, and high adsorption properties [23,25]. Hence, in this paper, the pechini sol-gel approach was used for the synthesis of MnFe_2O_4 nanoparticles using tartaric acid to serve as a chelating agent in addition to 1,2-propanediol to serve as a crosslinker. The synthesized MnFe_2O_4 nanoparticles were characterized using several tools such as Fourier-transform infrared spectroscopy (FTIR), X-ray diffraction (XRD), transmission scanning electron microscopy (TEM), energy-dispersive X-ray spectroscopy (EDS), and scanning electron microscopy (SEM). Further, the synthesized MnFe_2O_4 nanoparticles were utilized for the adsorption of safranin T dye from aqueous media. Also, the impacts of pH, contact time, temperature, concentration, and reusability were investigated. Manganese ferrite nanoparticles offer distinct advantages that render them appealing for safranin T dye removal. Being a magnetic material, these nanoparticles facilitate effortless separation from a solution through the application of an external magnetic field. This characteristic streamlines the recovery and reusability of the adsorbent, diminishing operational expenses and enhancing the environmental friendliness of the process. Moreover, manganese ferrite nanoparticles typically exhibit a substantial surface area, providing numerous active sites for adsorption and ensuring the efficient extraction of contaminants from a solution. Notably, these nanoparticles are recognized for their chemical stability, a pivotal attribute for effective adsorbents, enabling them to withstand diverse chemical conditions without significant degradation, thereby ensuring prolonged performance. Depending on the synthesis method and the availability of raw materials, MnFe_2O_4 nanoparticles may represent a cost-effective adsorbent compared to certain alternatives, making economic considerations paramount in the selection of adsorbents for large-scale applications.

2. Experimental

2.1. Materials

1,2-propanediol ($\text{C}_3\text{H}_8\text{O}_2$), iron(III) nitrate nonahydrate ($\text{Fe}(\text{NO}_3)_3 \cdot 9\text{H}_2\text{O}$), manganese(II) nitrate tetrahydrate ($\text{Mn}(\text{NO}_3)_2 \cdot 4\text{H}_2\text{O}$), hydrochloric acid (HCl), tartaric acid ($\text{C}_4\text{H}_6\text{O}_6$), sodium hydroxide (NaOH), potassium nitrate (KNO_3), and safranin T dye ($\text{C}_{20}\text{H}_{19}\text{ClN}_4$) were obtained from Sigma-Aldrich.

2.2. Synthesis of MnFe_2O_4 Nanoparticles

The manganese ferrite nanoparticles were synthesized by the pechini sol-gel method as the following; 80 mL of manganese aqueous solution, which contains 3.65 g of $\text{Mn}(\text{NO}_3)_2 \cdot 4\text{H}_2\text{O}$, was added to 80 mL of iron aqueous solution, which contains 11.75 g of $\text{Fe}(\text{NO}_3)_3 \cdot 9\text{H}_2\text{O}$. After that, 80 mL of chelating agent aqueous solution, which contains 5.09 g of tartaric acid, was added then the resulting mixture was continuously stirred for 10 min at room temperature. Additionally, 10 mL of 1,2-propanediol crosslinker was added then the resulting mixture was continuously stirred at 140 °C so that complete evaporation occurred. Finally, the remaining powder was calcinated at 670 °C for 3 h to produce manganese ferrite nanoparticles.

2.3. Characterization

The nature of the synthesized manganese ferrite nanoparticles was examined using the D8 advance diffractometer (Billerica, MA, USA) and $\text{CuK}\alpha$ radiations with a wavelength (λ) of 1.5402 Å. Utilizing the Shimadzu spectrometer, Fourier transforms infrared spectrophotometer (Kyoto, Japan) was applied to investigate the functional groups of manganese ferrite nanoparticles. The surface morphology and composition of the manganese ferrite nanoparticles were examined using scanning electron microscopy (SEM, FEI Nova Nano SEM450 instrument, Waltham, MA, USA) attached to energy-dispersive X-ray analysis (EDS). The morphology of the manganese ferrite nanoparticles was examined using transmission electron microscopy (TEM, JEOL JEM 2100F instrument, Akishima, Tokyo, Japan). The BET surface area of the manganese ferrite nanoparticles was determined using an N_2 gas sorption analyzer (Quantachrome, Model: TouchWin, Graz, Austria).

2.4. Adsorption of Safranin T Dye from Aqueous Solutions

An amount of 50 mg of synthesized nanoadsorbent (manganese ferrite nanoparticles) was added to 100 mL of safranin T dye solution to study several factors such as pH, time, temperature, and concentration, according to the experimental conditions in Table 1. Afterward, the adsorbent was separated with a magnet, and the remaining safranin T dye concentration in the filtrate was measured at 530 nm using a Shimadzu 1800 series UV-Vis spectrophotometer (Kyoto, Japan).

Table 1. Experimental terms for the adsorption of safranin T dye using manganese ferrite nanoparticles.

Effect	Concentration of Safranin T Dye (mg/L)	Volume of Safranin T Dye (mL)	Amount of Adsorbent (g)	Temperature (K)	Time (min)
pH (2–8)	200	100	0.05	298	180
Time (10–120 min)	200	100	0.05	298	10–120
Temperature (298–328 K)	200	100	0.05	298–328	80
Concentration (50–300 mg/L)	50–300	100	0.05	298	80

The removal efficiency (% R) and the amount of safranin T dye removed by the manganese ferrite nanoparticles were calculated applying Equations (1) and (2), respectively [23,25].

$$\% R = \frac{C_o - C_e}{C_o} \times 100 \quad (1)$$

$$Q = (C_o - C_e) \times \frac{V}{M} \quad (2)$$

C_o corresponds to the initial concentration of safranin T dye (mg/L), whereas C_e corresponds to the equilibrium concentration of safranin T dye (mg/L). M corresponds to the weight of the manganese ferrite nanoparticles (g), whereas V corresponds to the volume of the safranin T dye solution (L).

The point zero charge (pH_{pzc}) of manganese ferrite nanoparticles was estimated through the solid addition procedure by adding 0.50 g of the manganese ferrite nanoparticles in 50 mL of 0.015 M of KCl solutions in several tightly sealed conical flasks. After that, the pH value is altered between 2.5 and 11.5 using 0.1 M HCl or NaOH and kept under stirring for 6 h at room temperature. The final pH (pH_f) was determined and plotted against the initial pH (pH_i). The pH_{pzc} of manganese ferrite nanoparticles was determined as the pH_f value at which a unique level was observed [23,25].

3. Results and Discussion

3.1. Synthesis and Characterization of $MnFe_2O_4$ Nanoparticles

In the pechini sol–gel method, to obtain pure $MnFe_2O_4$ nanoparticles without other phases, Fe(III) and Mn(II) ions (molar ratio of Mn(II)/Fe(III) = 1/2) react with tartaric acid (molar ratio of tartaric acid/Fe(III) = 3/2, whereas the molar ratio of tartaric acid/Mn(II) = 1/1), which acts as a chelating agent, to form ferric tartrate and manganese tartrate chelates, as shown in Scheme 1. Next, the resulting chelates react with 1,2-propanediol, which acts as a crosslinker, to form large networks that burn at 670 to give $MnFe_2O_4$ nanoparticles, as shown in Scheme 1. It is worth noting that thermal examination of the formed powder prior to calcination showed that 670 °C is the ideal temperature at which $MnFe_2O_4$ nanoparticles with small crystal size are formed, as shown in Figure 1.

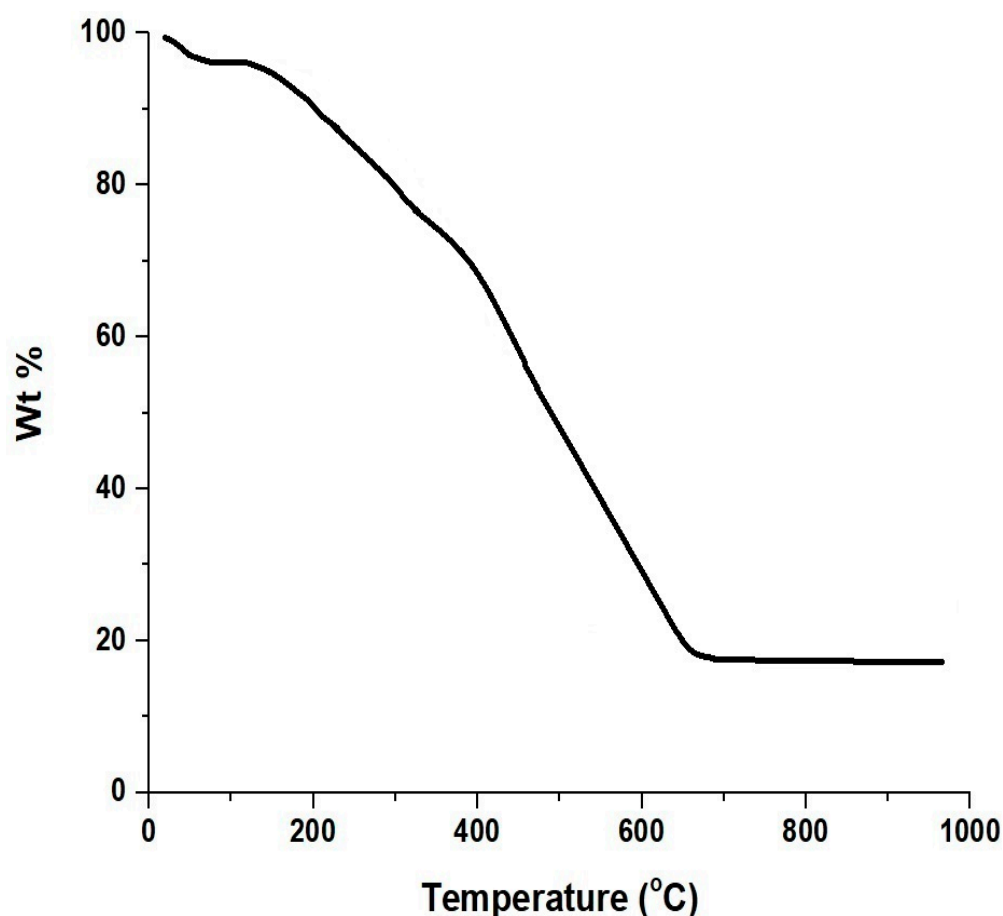


Figure 1. Thermal gravimetric analysis of the formed powder by the pechini sol–gel method before the calcination process.

Figure 2A illustrates the XRD spectrum of $MnFe_2O_4$ nanoparticles, showcasing distinct diffraction peaks located at specific 2θ values of 18.17° , 30.03° , 35.49° , 37.07° , 43.16° , 53.54° , 57.11° , 62.87° , 71.27° , 74.22° , 75.15° , and 79.26° . These peaks match the crystal planes (111), (220), (311), (222), (400), (442), (511), (440), (620), (533), (622), and (444), respectively. The identification aligns with data from JCPDS database No. 38-0430 [34]. Additionally, the Debye-Scherrer formula estimated the average crystal size to be approximately 18.89 nm. The crystal system, lattice constant, and space group of synthesized $MnFe_2O_4$ nanoparticles are cubic, 0.844 nm, and $Fd\bar{3}m$, respectively.

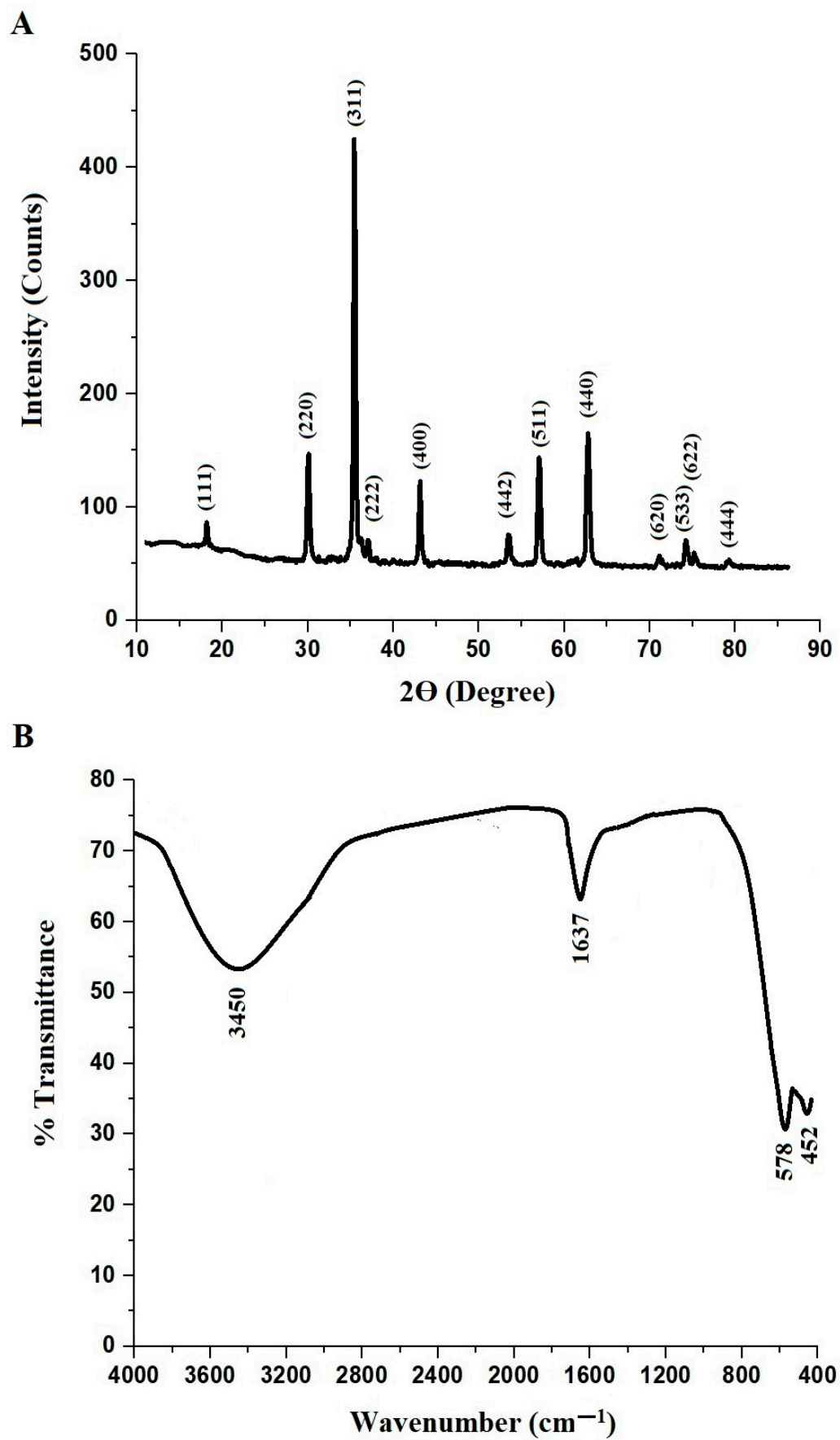


Figure 2. XRD (A) and FTIR (B) analyses of MnFe_2O_4 nanoparticles.

The FT-IR spectrum of MnFe_2O_4 nanoparticles is displayed in Figure 2B. The spectrum exhibits two main absorption bands under 1000 cm^{-1} , a common feature of metal ferrites. The absorption peaks at 578 and 452 cm^{-1} may be attributed to the Mn–O and Fe–O stretching vibrations of MnFe_2O_4 nanoparticles, respectively. The bands at 3450 and 1637 cm^{-1} may be ascribed to the stretching and bending vibrations of hydroxyl groups or O–H surface water molecules, respectively [34].

The surface morphology and average grain size of the MnFe_2O_4 nanoparticles were indicated by the SEM image and its histogram, as shown in Figure 3A,B, respectively. Consequently, semi-spherical particles with a mean grain size of 134.25 nm are clearly observed. Further, the morphology and average particle size of the MnFe_2O_4 nanoparticles were indicated by the TEM image and its histogram, as shown in Figure 4A,B, respectively. The shape of MnFe_2O_4 nanoparticles is semi-spherical, with an average particle size of 19.32 nm that coincides well with that measured from the XRD results.

The composition of the MnFe_2O_4 nanoparticles has been identified using the EDX technique, and the pattern produced is displayed in Figure 5A, which indicates the presence of Fe (49.12%), Mn (17.63%), and O (33.25%) peaks only. The magnetic properties of MnFe_2O_4 nanoparticles were recorded at room temperature using a vibrating sample magnetometer, and the hysteresis curve of the nanoparticles is shown in Figure 5B. The results showed that the saturation magnetization is 15.35 emu/g .

3.2. Safranin T Dye Removal from Aqueous Solutions

3.2.1. Influence of pH

Figure 6A demonstrates the influence of dye solution pH on the removal percentage (% R) of safranin T dye. The safranin T dye removal percentage experienced an upward trend with the rise in pH within the aqueous solution range from 2 to 8. Specifically, the removal percentage of safranin T dye showed an escalation from 2.58% at pH 2 to 80.94% at pH 8. This shift is attributed to the neutral charge of the manganese ferrite surface (pH_{pzc}), which is determined to be 4.65, as depicted in Figure 6B. If the pH is below the pH_{pzc} , the surface of manganese ferrite nanoparticles carries a positive charge, leading to electrostatic repulsion with the cationic safranin T dye. Conversely, at pH levels exceeding the pH_{pzc} , the surface of manganese ferrite nanoparticles becomes negatively charged, fostering increased adsorption of positively charged safranin T dye species [23,25].

MnFe_2O_4 nanoparticles with a small crystalline size (18.89 nm) were formed at a calcination temperature of $670\text{ }^\circ\text{C}$, as shown in Figure 1. Raising the calcination temperature to $800\text{ }^\circ\text{C}$ led to the formation of MnFe_2O_4 nanoparticles with a large crystal size (60.65 nm) (XRD figure omitted for brevity). Higher calcination temperatures can accelerate the rate of crystal growth, ensuring the formation of larger crystals. The BET surface areas of the MnFe_2O_4 nanoparticles, which were synthesized at 670 and $800\text{ }^\circ\text{C}$, are 135.68 and $65.72\text{ m}^2/\text{g}$, respectively. The removal percentages of safranin T dye using the MnFe_2O_4 nanoparticles, which were synthesized at 670 and $800\text{ }^\circ\text{C}$, at pH 8 are 80.94 and 40.26%, respectively. This can be explained based on the inverse relationship between the BET surface area and the removal percentage of safranin T dye. Hence, the sample calcinated at $670\text{ }^\circ\text{C}$ was selected for adsorption study because it has a smaller crystalline size and a higher surface area, which makes it more effective in removing safranin T Dye from aqueous media. Small crystalline particles generally have a higher surface area compared to larger ones. Adsorption occurs at the surface of materials, and a larger surface area provides more sites for adsorption to take place. This means that more molecules of the adsorbate can interact with the material, leading to higher adsorption capacity.

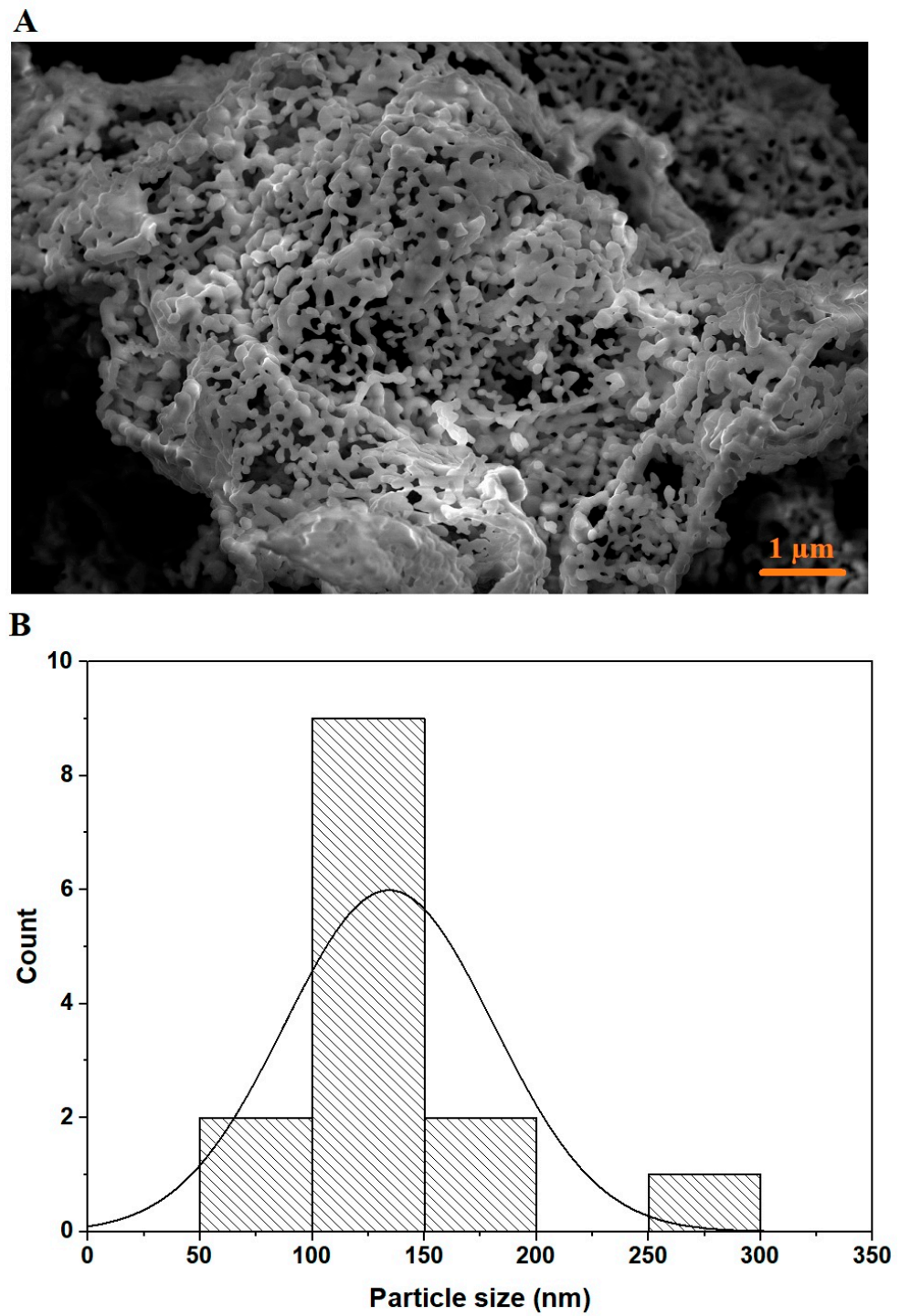


Figure 3. SEM (A) and its histogram (B) of MnFe_2O_4 nanoparticles.

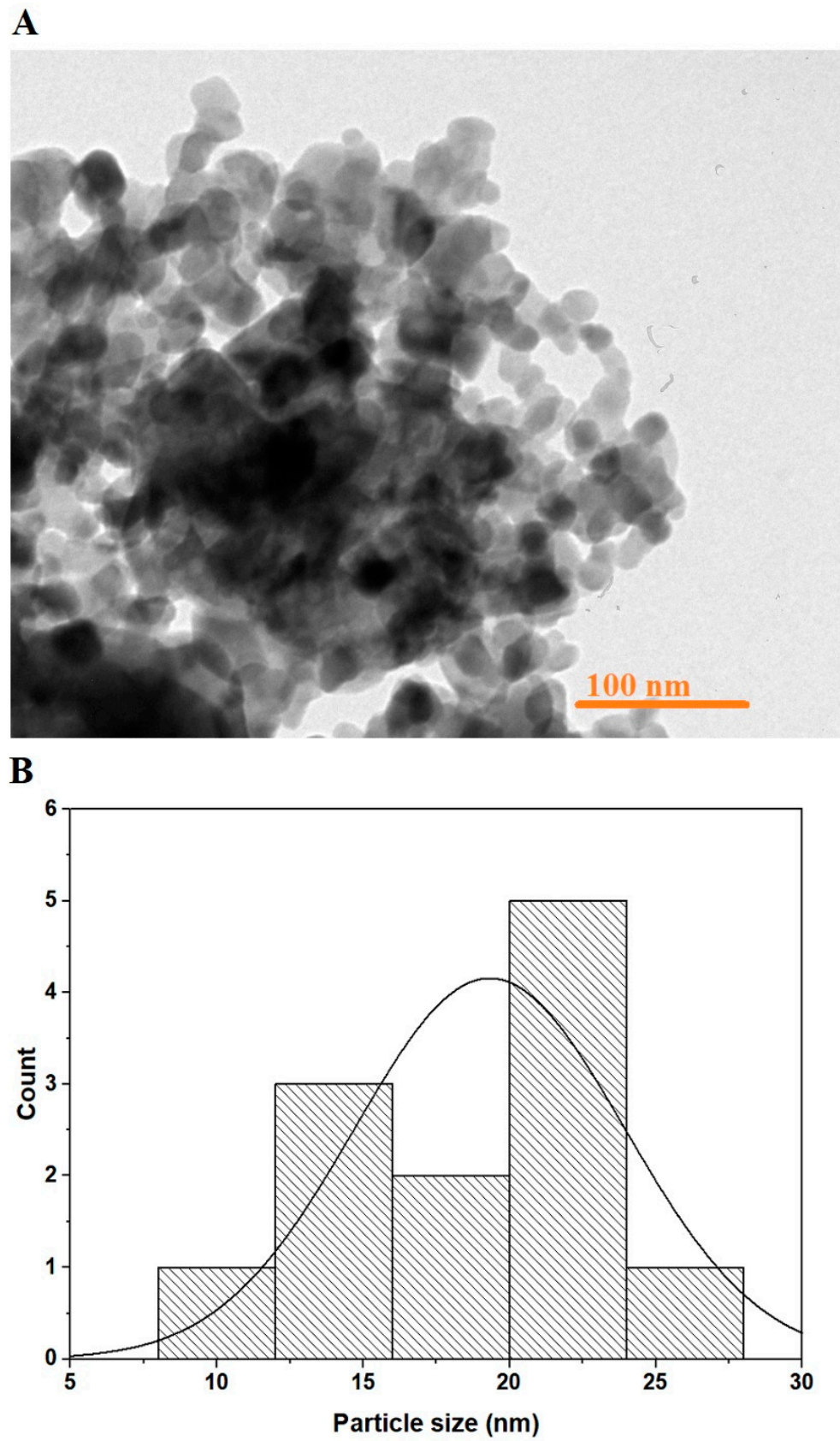


Figure 4. TEM (A) and its histogram (B) of MnFe_2O_4 nanoparticles.

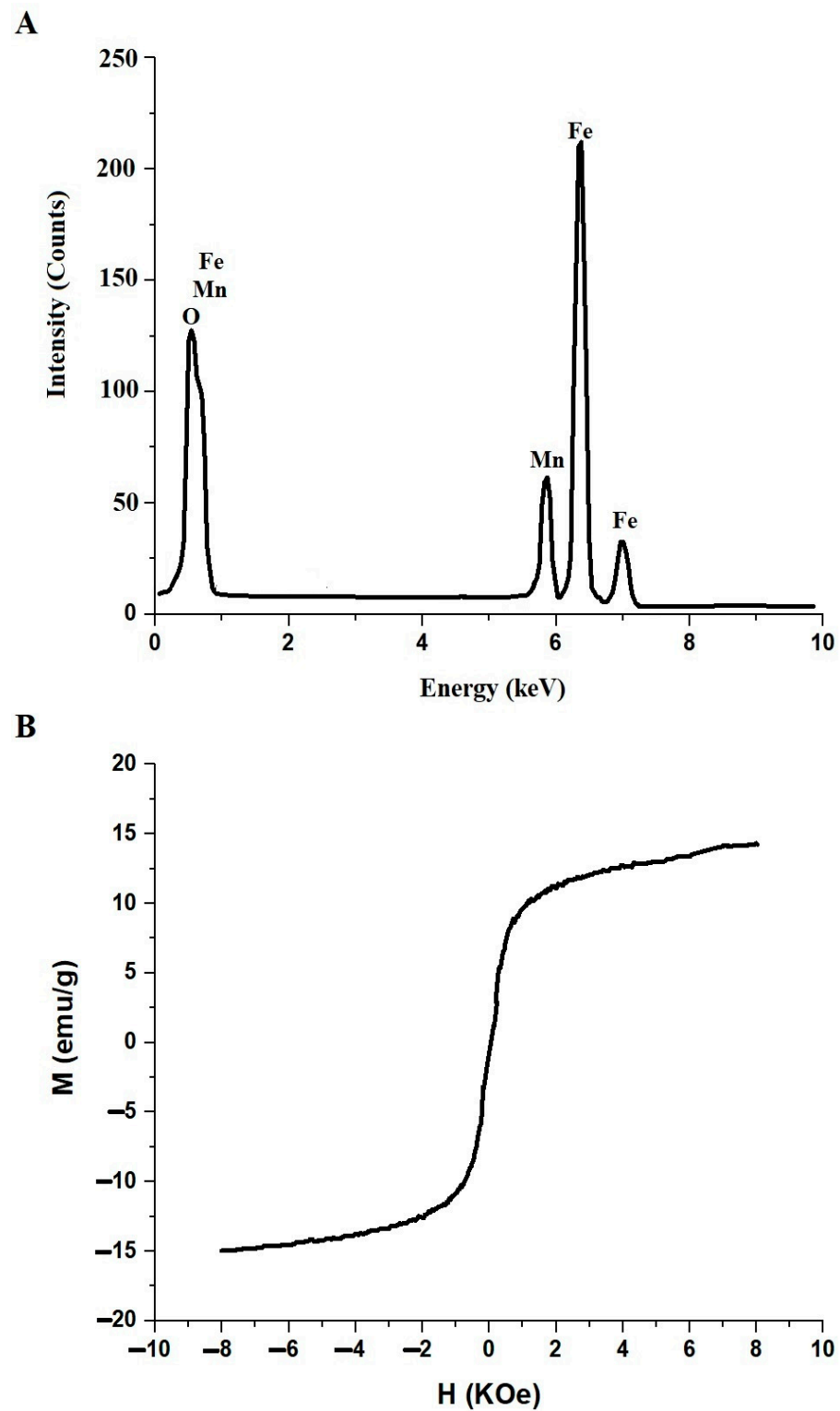


Figure 5. EDS (A) and magnetic (B) analyses of MnFe_2O_4 nanoparticles.

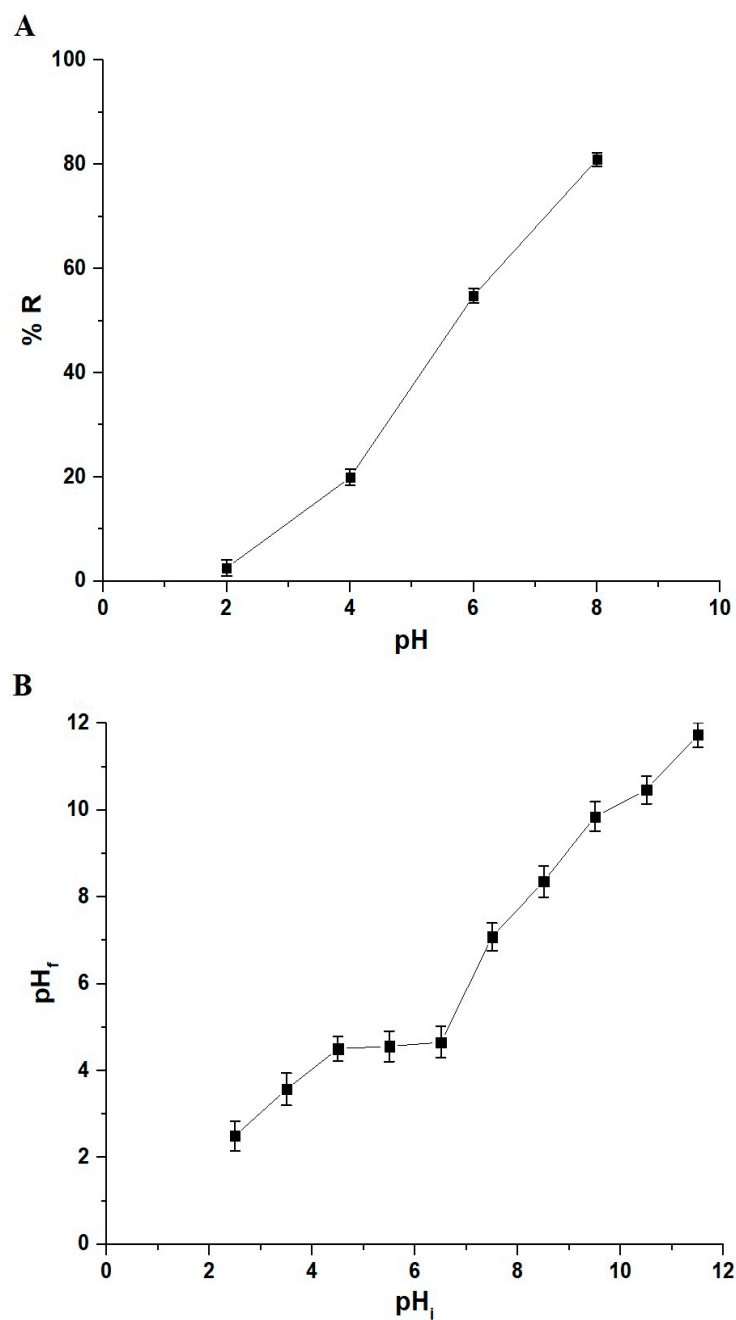


Figure 6. Influence of pH on the sorption of safranin T dye on manganese ferrite nanoparticles (A). Plot for the estimation of pH_{pzc} for the manganese ferrite nanoparticles (B).

Figure 3A displays the semi-spherical shapes of the $MnFe_2O_4$ nanoparticles before the adsorption process. After the adsorption of safranin T dye, as depicted in Figure 7A, obvious changes in the surface morphology of the $MnFe_2O_4$ nanoparticles were noticed in the SEM image. The adsorbate, referring to the material that endured adsorption, was attached to the surface of the adsorbent, displaying itself as a deposit or coating. To confirm the adsorption of safranin T dye by the produced adsorbent, FT-IR analysis was carried out after the adsorption of safranin T dye, as demonstrated in Figure 7B. The new band at 1591 cm^{-1} is due to the stretching vibration of C=C aromatic of safranin T dye. In addition, the new bands located at 2901 and 3106 cm^{-1} are due to the stretching vibrations of the aliphatic and aromatic CH of safranin T dye, respectively. In addition, the presence of multiple new bands in the region $690\text{--}850\text{ cm}^{-1}$ is due to aromatic CH out of plane bending vibration.

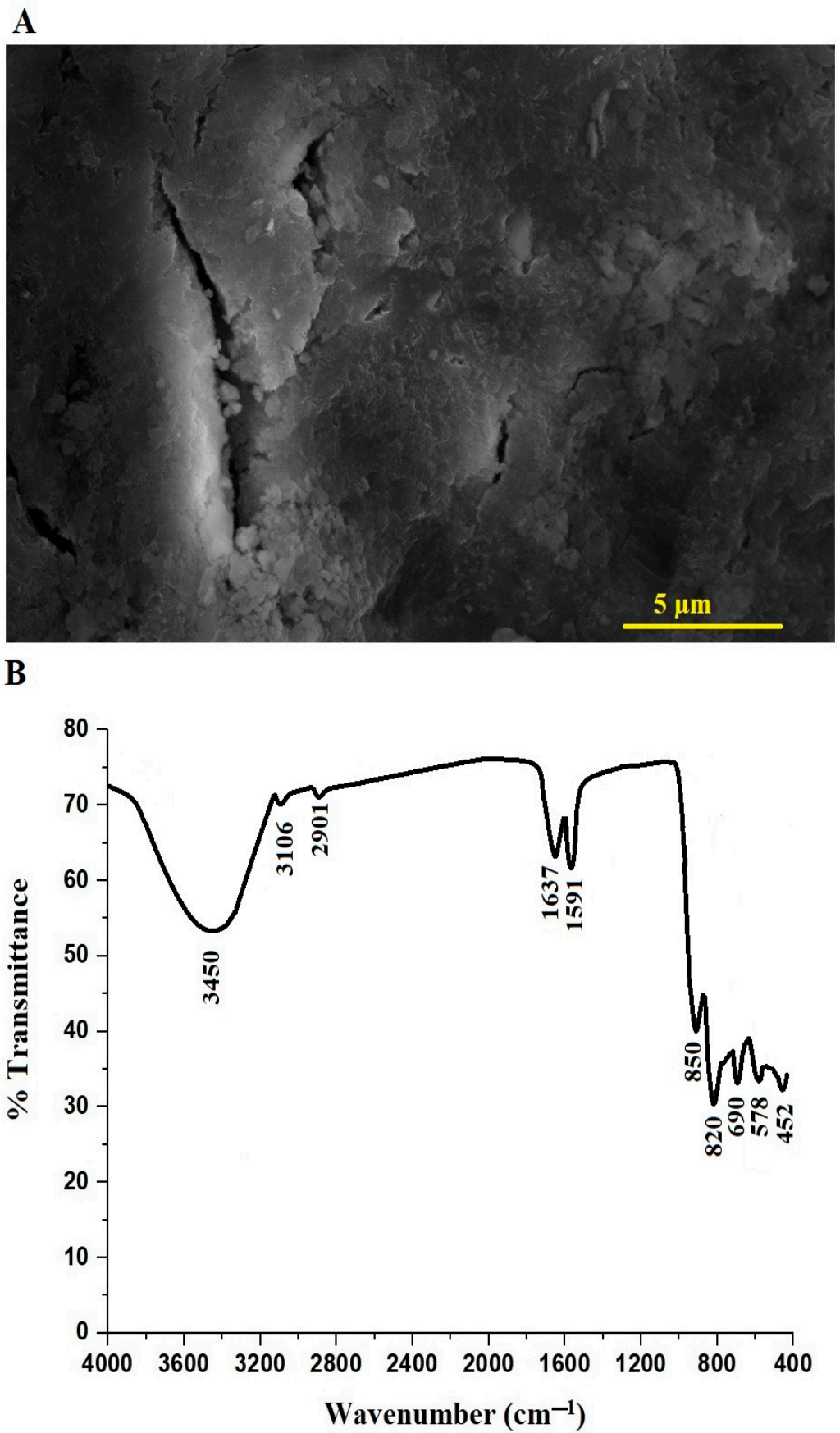


Figure 7. SEM (A) and FTIR analyses (B) of the MnFe_2O_4 nanoparticles after the adsorption of safranin T dye.

3.2.2. Influence of Adsorption Time and Adsorption Kinetics

Figure 8A illustrates the influence of time on the removal percentage (% R) of safranin T dye. The safranin T dye removal percentage experienced an upward trend with the rise in time within the range from 10 to 80 min. Specifically, the removal percentage of safranin T dye showed an escalation from 29.87% after 10 min to 80.18% after 80 min due to the presence of available active sites. Further, there is an approximate stability in the removal percentage of safranin T dye with increasing time from 80 to 120 min due to the saturation of active sites. The pseudo-first-order (Equation (3)) and pseudo-second-order (Equation (4)) kinetic sorption models were utilized to estimate the experimental results and clarify the adsorption mechanism [23,25].

$$\log(Q_e - Q_t) = \log Q_e - \frac{K_1}{2.303}t \quad (3)$$

$$\frac{t}{Q_t} = \frac{1}{K_2 Q_e^2} + \frac{1}{Q_e}t \quad (4)$$

K_1 (1/min) and Q_e (mg/g) refers to the pseudo-first-order rate constant and the amount of safranin T dye adsorbed at equilibrium, respectively. K_2 (g/mg.min) and Q_t (mg/g) refers to the rate constant of pseudo-second-order and the amount of safranin T dye adsorbed at any time, respectively. Moreover, kinetic constants from the linear regression plots are listed in Table 2. Figure 8B,C shows the pseudo-first-order and pseudo-second-order for the sorption of safranin T dye onto the manganese ferrite nanoparticles, respectively. The findings indicate that the adsorption capacity determined through the pseudo-second-order model closely aligns with the experimental adsorption capacity (Q_{exp}). Additionally, the correlation coefficient (R^2) obtained from the pseudo-second-order model surpasses that obtained from the pseudo-first-order model. Consequently, the kinetics of safranin T dye on manganese ferrite nanoparticles can be effectively explained through the pseudo-second-order kinetic model.

Table 2. Kinetics constants for the adsorption of safranin T dye by the manganese ferrite nanoparticles.

Experimental Q_{exp} (mg/g)	Pseudo-First-Order			Pseudo-Second-Order		
	Q_e (mg/g)	K_1 (1/min)	R^2	Q_e (mg/g)	K_2 (g/mg.min)	R^2
320.7	228.57	0.0210	0.9724	322.58	0.00018	0.9993

3.2.3. Influence of Solution Temperature and Thermodynamic Constants

Figure 9A illustrates the influence of temperature on the removal percentage (% R) of safranin T dye. The safranin T dye removal percentage experienced a decreasing trend with the rise in temperature within the range from 298 to 328 K. The thermodynamic constants such as entropy change (ΔS°), enthalpy change (ΔH°), and free energy change (ΔG°) were identified using Equations (5)–(7) [23,25].

$$\ln K_T = \frac{\Delta S^\circ}{R} - \frac{\Delta H^\circ}{RT} \quad (5)$$

$$\Delta G^\circ = \Delta H^\circ - T\Delta S^\circ \quad (6)$$

$$K_T = \frac{Q_e}{C_e} \quad (7)$$

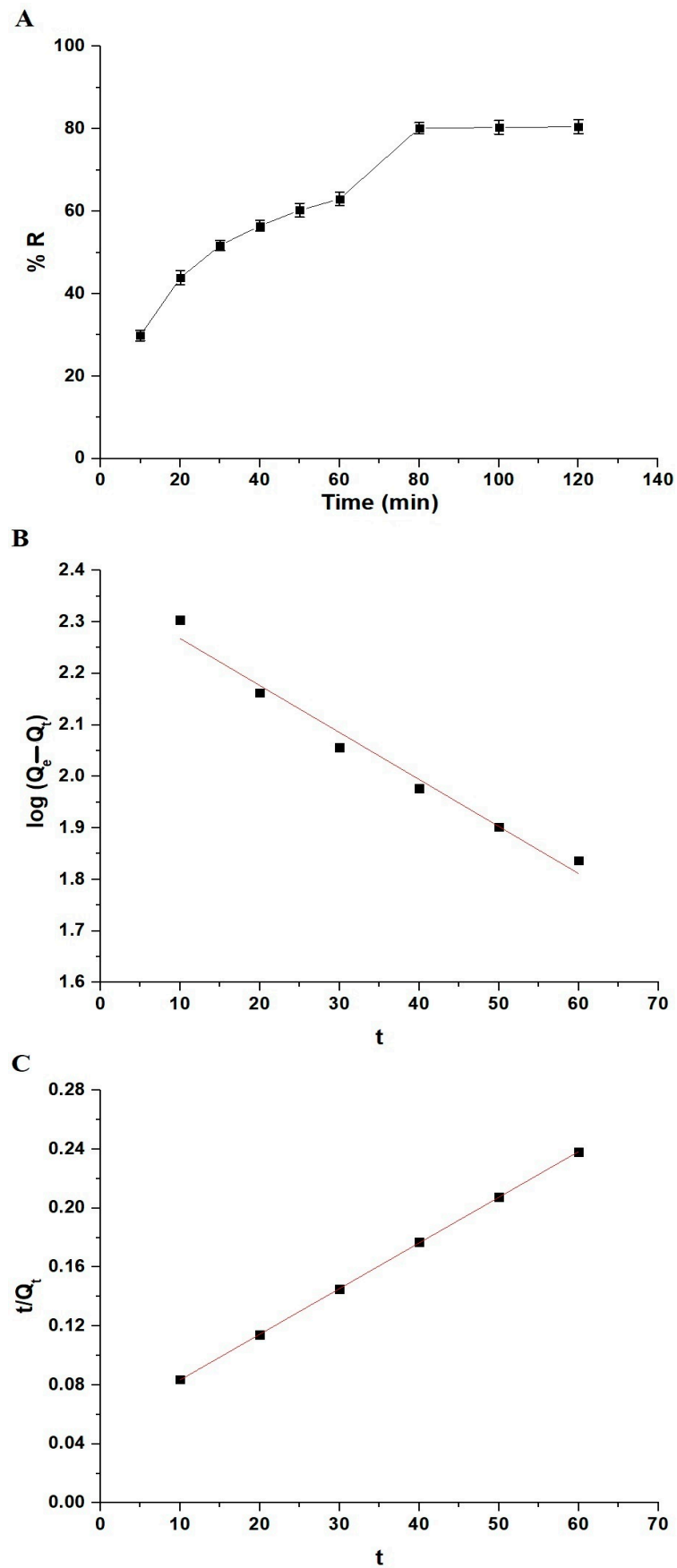


Figure 8. Influence of time on the sorption of safranin T dye on manganese ferrite nanoparticles (A). The pseudo-first-order (B) and pseudo-second-order (C) kinetic sorption models.

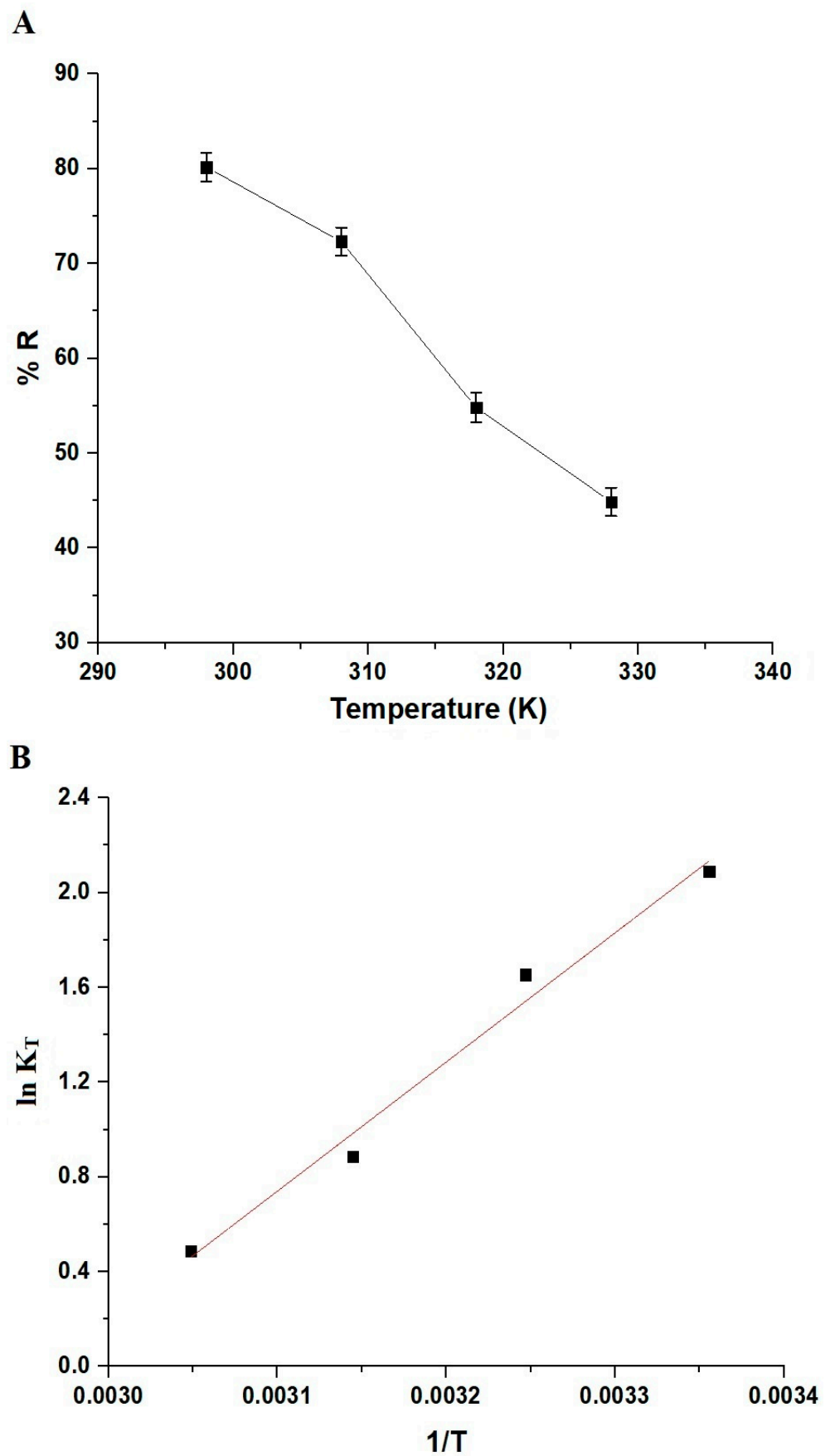


Figure 9. Impact of dye solution temperature on the sorption of safranin T dye on manganese ferrite nanoparticles (A). The representation of $\ln K_T$ against $1/T$ (B).

K_T refers to the distribution coefficient (L/g). T refers to the removal temperature (K), whereas R refers to the ideal gas constant in KJ/molK unit. The values of ΔH° and ΔS° were computed from the slope and intercept of the linear regression of $\ln K_T$ versus $1/T$, as shown in Figure 9B. The values of ΔS° , ΔH° , and ΔG° are revealed in Table 3. The positive value of the entropy change indicates the affinity of the manganese ferrite nanoparticles towards safranin T dye. The negative sign and value of the enthalpy change confirmed that the removal process of safranin T dye onto manganese ferrite nanoparticles is exothermic and chemical. Further, the negative values of free energy change demonstrated that the removal process of safranin T dye onto manganese ferrite nanoparticles is spontaneous.

Table 3. Calculated thermodynamic parameters of safranin T dye sorption onto manganese ferrite nanoparticles.

ΔH° (KJ/mol)	ΔS° (KJ/molK)	ΔG° (KJ/mol)			
		298	308	318	328
−45.56	0.1350	−85.80	−87.15	−88.50	−89.85

3.2.4. Influence of Initial Safranin T Dye Concentration and Adsorption Equilibrium Isotherms

Figure 10A illustrates the influence of initial dye concentration on the removal percentage (% R) of safranin T dye. The safranin T dye removal percentage experienced a decreasing trend with the rise in concentration within the range from 50 to 300 mg/L.

The Langmuir (Equation (8)) and Freundlich (Equation (9)) equilibrium sorption isotherms were studied to estimate the experimental results and clarify the adsorption mechanism [23,25].

$$\frac{C_e}{Q_e} = \frac{1}{K_3 Q_{\max}} + \frac{C_e}{Q_{\max}} \quad (8)$$

$$\ln Q_e = \ln K_4 + \frac{1}{n} \ln C_e \quad (9)$$

Q_{\max} refers to the maximum adsorption capacity (mg/g), whereas K_3 refers to the Langmuir constant (L/mg). $1/n$ refers to the degree of heterogeneity, whereas K_4 refers to the Freundlich constant (mg/g)(L/mg)^{1/n}. It is important to mention that Q_{\max} can be computed from Freundlich isotherm using Equation (10) [23,25].

$$Q_{\max} = K_4 \left(C_o^{1/n} \right) \quad (10)$$

Moreover, equilibrium constants from the linear regression plots are listed in Table 4. Figure 10B,C shows the Langmuir and Freundlich isotherms for the sorption of safranin T dye onto the manganese ferrite nanoparticles, respectively.

Table 4. Langmuir and Freundlich constants for the removal of safranin T dye by the manganese ferrite nanoparticles.

Langmuir Isotherm			Freundlich Isotherm		
Q_{\max} (mg/g)	K_3 (L/mg)	R^2	Q_{\max} (mg/g)	K_4 (mg/g)(L/mg) ^{1/n}	R^2
334.45	0.3229	0.9996	426.99	112.43	0.7465

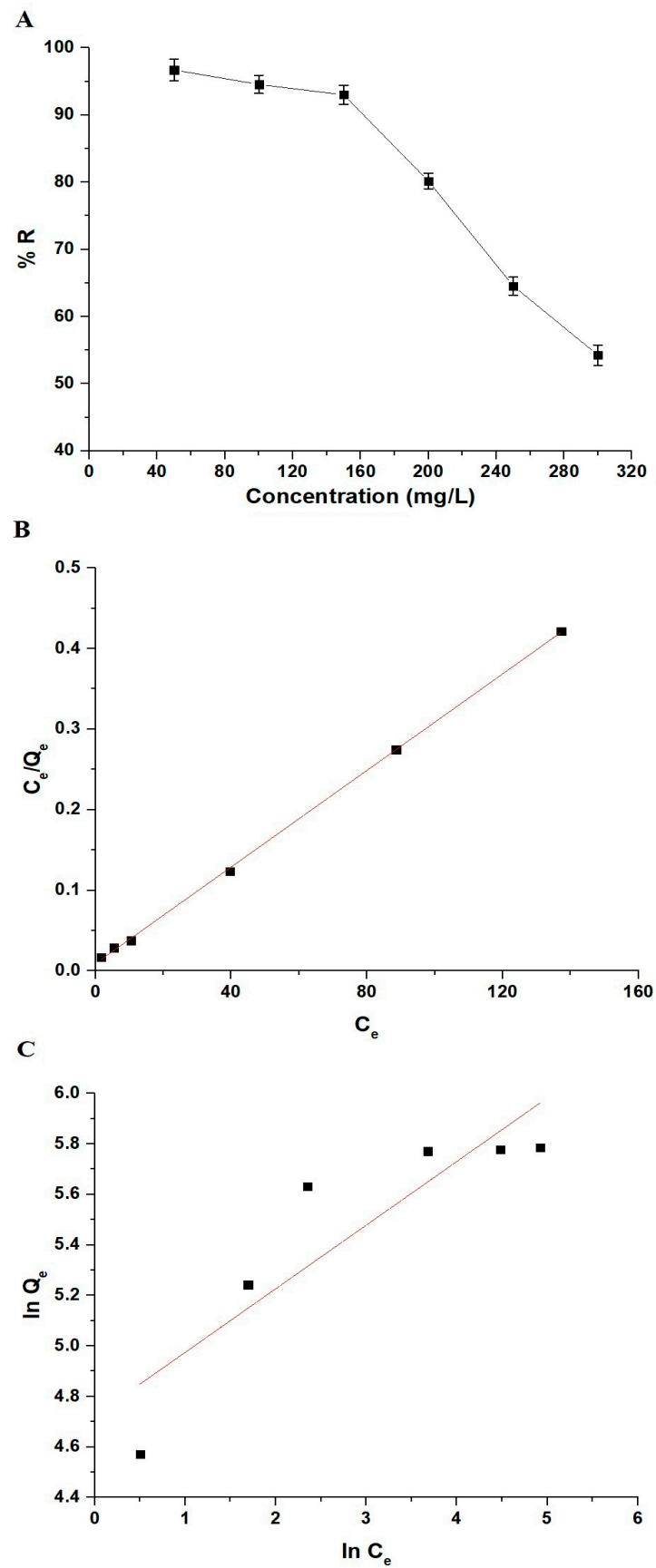


Figure 10. Influence of concentration on the sorption of safranin T dye on manganese ferrite nanoparticles (A). The applied Langmuir (B) and Freundlich (C) sorption equilibrium isotherms.

Also, Dubinin–Radushkevich (Equation (11)) and Temkin (Equation (12)) isotherms were studied, as shown in Figure 11A,B, respectively [35].

$$\ln Q_e = \ln Q_{\max} + K_5 \varepsilon^2 \quad (11)$$

$$Q_e = B \ln K_6 + B \ln C_e \quad (12)$$

K_5 refers to the Dubinin–Radushkevich constant (mol^2/KJ^2), whereas ε refers to the Polanyi potential which is determined using Equation (13).

$$\varepsilon = RT \ln \left(\frac{1}{1 + C_e} \right) \quad (13)$$

K_6 refers to the Temkin constant related to equilibrium bonding (L/g), whereas B refers to the Temkin constant related to the heat of adsorption.

Moreover, equilibrium constants from the linear regression plots are listed in Table 5.

Table 5. Dubinin–Radushkevich and Temkin constants for the removal of safranine T dye by the manganese ferrite nanoparticles.

Dubinin–Radushkevich Isotherm			Temkin Isotherm		
Q_{\max} (mg/g)	K_5 (mol^2/KJ^2)	R^2	B	K_6 (L/g)	R^2
150.17	0.00636	0.5007	50.80	8.11	0.8317

It was founded that the correlation coefficient of the Langmuir isotherm is higher than that of the other isotherms such as Dubinin–Radushkevich, Freundlich, and Temkin. Hence, the removal of safranine T dye on the manganese ferrite nanoparticles fitted well with the Langmuir rather than the other applied isotherms.

Table 6 presents a comparative analysis of the adsorption capacity of manganese ferrite nanoparticles in relation to other reported adsorbents such as magnetic graphene oxide-containing chitosan-sodium alginate hydrogel, magnetic mesoporous clay, carboxy methyl cellulose incorporated acrylic hydrogels, clinoptilolite, phillipsite, heulandite, modified bituminous activated carbon with nitric acid, modified bituminous activated carbon with zinc oxide, and porous graphite [6,36–39]. Upon examination of the table, it becomes evident that the adsorption capacity of manganese ferrite nanoparticles surpasses that of the majority of established adsorbents. Consequently, manganese ferrite nanoparticles exhibit considerable promise as a material for the removal of safranine T dye from contaminated aqueous media. Manganese ferrite nanoparticles have certain advantages that make them attractive for removing safranine T dye. Manganese ferrite nanoparticles are a magnetic material that allows for easy separation from a solution using an external magnetic field. This property simplifies the recovery and reuse of the adsorbent, reducing operational costs and making the process more environmentally friendly. Manganese ferrite nanoparticles typically have a high surface area. A high surface area provides more active sites for adsorption, allowing for the efficient removal of contaminants from a solution. Manganese ferrite nanoparticles are known for their chemical stability, which is an important factor for adsorbents. It can withstand a range of chemical conditions without undergoing significant degradation, ensuring its performance over time. Depending on the synthesis method and availability of raw materials, MnFe_2O_4 nanoparticles may be a cost-effective adsorbent compared to some alternatives. Economic considerations are crucial when selecting an adsorbent for large-scale applications.

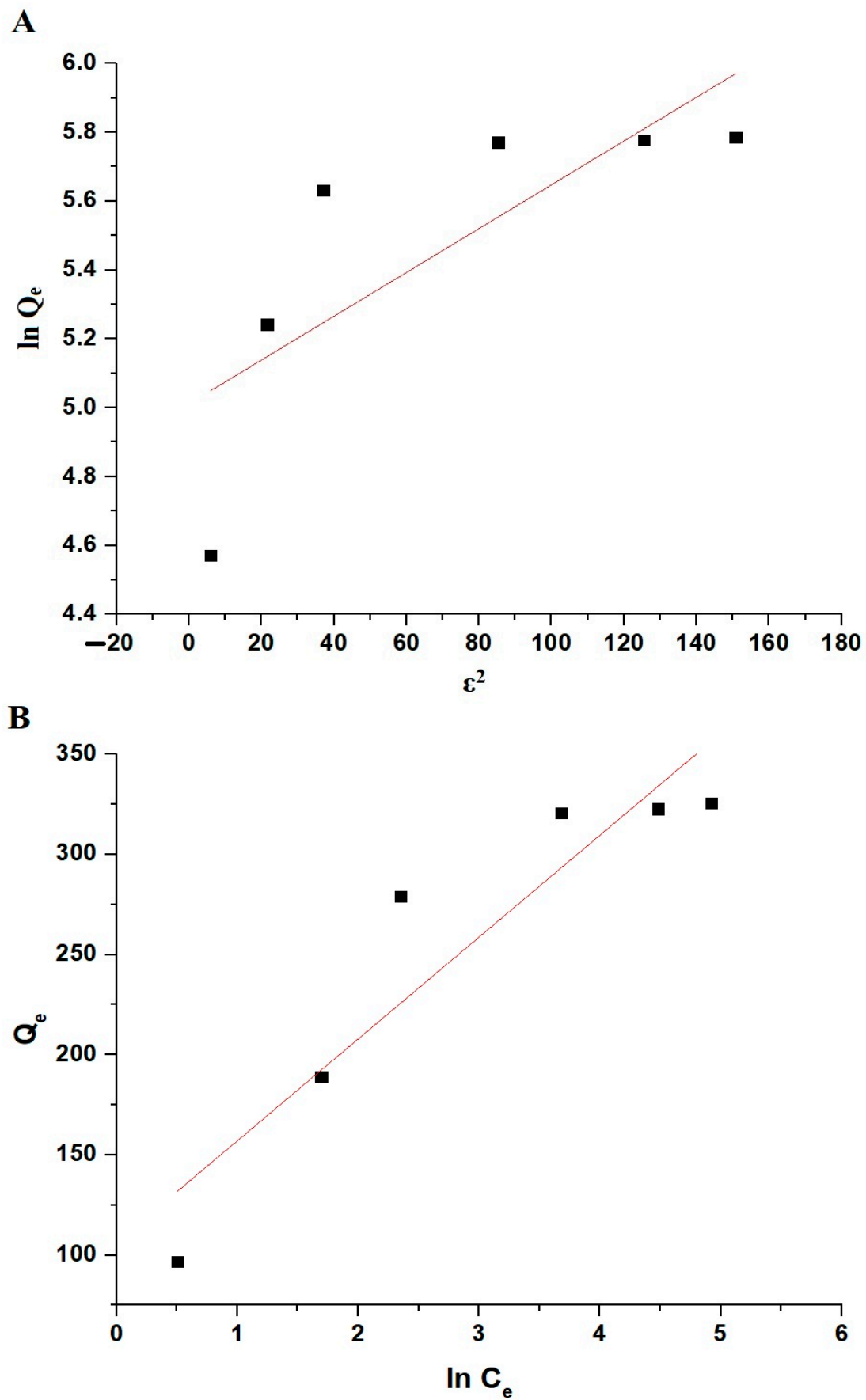


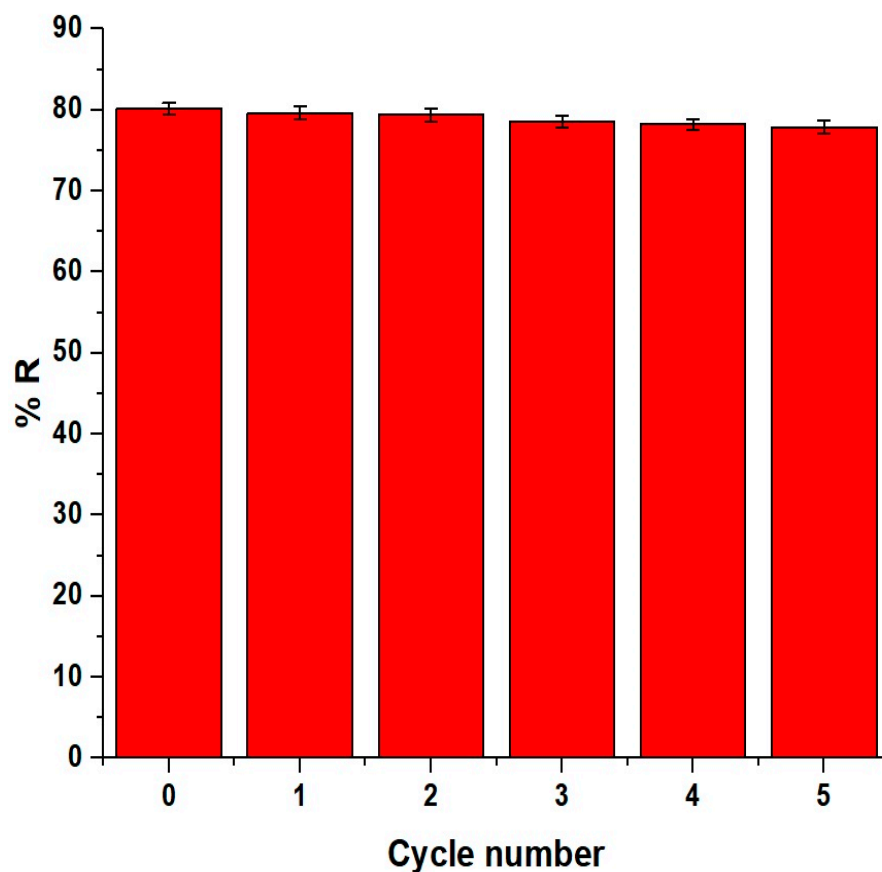
Figure 11. The applied Dubinin–Radushkevich (A) and Temkin (B) sorption equilibrium isotherms.

Table 6. Comparison of the sorption capacities of various sorbents towards safranin T dye.

Adsorbents	Maximum Sorption Capacity (mg/g)	Ref.
Magnetic graphene oxide-containing chitosan-sodium alginate hydrogel	44.313	[6]
Magnetic mesoporous clay	37.97	[36]
Carboxy methyl cellulose incorporated acrylic hydrogels	63.25	[37]
Clinoptilolite	42.90	[38]
Phillipsite	65.35	[38]
Heulandite	41.66	[38]
Modified bituminous activated carbon with nitric acid	27.40	[39]
Modified bituminous activated carbon with zinc oxide	32.46	[39]
Porous graphite	33.67	[39]
MnFe ₂ O ₄ nanoparticles	334.45	This study

3.2.5. Influence of Renewal and Reusability

For the renewal of MnFe₂O₄ nanoparticles, the MnFe₂O₄/safranin T dye blend underwent heating at 600 °C, causing the breakdown and removal of the safranin T dye. Following this, the regenerated MnFe₂O₄ nanoadsorbent was employed for the sequential adsorption of safranin T dye through five successive cycles and presented in Figure 12, adhering to the identical experimental procedure outlined earlier. The results demonstrated the MnFe₂O₄ nanoparticles' ability to consistently eliminate safranin T dye without encountering a substantial decrease in effectiveness.

**Figure 12.** Impact of reusability process of MnFe₂O₄ nanoparticles for the removal of safranin T dye.

To confirm the stability of the MnFe_2O_4 nanoparticles, XRD of the regenerated MnFe_2O_4 nanoparticles after the fifth cycle was carried out and the results displayed that there were no differences in the positions or intensities of peaks, as shown in Figure 13. Hence, the reuse of adsorbent aligns with sustainability goals by promoting resource efficiency and reducing the need for continuous production and disposal of adsorbent materials. This is particularly important in the context of environmentally conscious practices.

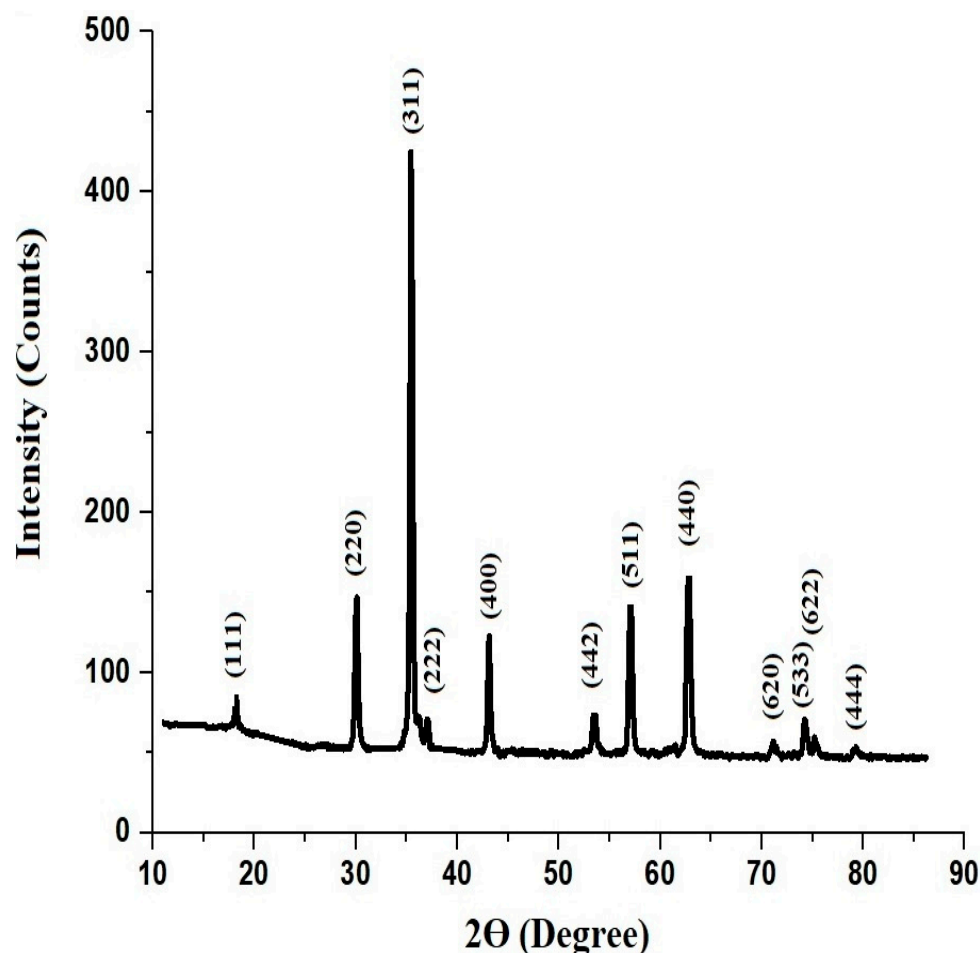


Figure 13. XRD of the regenerated MnFe_2O_4 nanoparticles after the fifth cycle.

3.2.6. Influence of Selectivity

In order to investigate the influence of several cations and anions on the removal efficiency of safranin T dye by MnFe_2O_4 nanoparticles, the interfering ion of concern was introduced at various concentrations into a 100 mL solution containing 200 $\mu\text{g}/\text{L}$ of the specific safranin T dye solution. The removal process was carried out according to the previously described protocol, and the removal percentage of safranin T dye was determined. The maximum concentration of the interfering ion that caused a 5% error in the removal percentage of safranin T dye was identified as the tolerance limit. Table 7 clearly indicates that most interfering ions exhibit a relatively high tolerance limit, demonstrating the selectivity of MnFe_2O_4 nanoparticles to remove safranin T dye.

Table 7. Removal of safranin T dye from binary mixtures in the presence of some interfering ions.

Interfering Ion	Tolerance Limit ($\mu\text{g/L}$)
K(I)	1000
Na(I)	1100
Ca(II)	105
Mg(II)	110
Cd(II)	80
Ni(II)	90
SO_4^{2-}	1450
CO_3^{2-}	1450

4. Conclusions

An effective removal method for safranin T dye from aqueous media was implemented operating easily produced manganese ferrite (MnFe_2O_4) nanoparticles. The synthesis of the manganese ferrite nanoparticles was carried out through the pechini sol–gel approach, employing tartaric acid to serve as a chelating agent in addition to 1,2-propanediol to serve as a crosslinker. According to TEM analysis, the MnFe_2O_4 nanoparticles exhibit semi-spherical particles with a mean size of 19.32 nm, aligning closely with the measurement obtained from XRD (18.89 nm). The maximum adsorption capacity of MnFe_2O_4 nanoparticles for safranin T dye reached 334.45 mg/g. The removal mechanism of safranin dye by manganese ferrite nanoparticles was found to be chemical, exothermic, and well described by the Langmuir equilibrium sorption isotherm as well as the pseudo-second-order kinetic model. Importantly, the synthesized manganese ferrite nanoparticles exhibited the ability to be reused multiple times without a significant loss of efficiency. The findings of this research suggest that MnFe_2O_4 nanoparticles could serve as a cost-effective, promising, sustainable, and efficient adsorbent for the removal of safranin T dye from aqueous solutions.

Author Contributions: Z.A., writing—review and editing (equal), conceptualization (equal), and methodology (equal); E.A.A., writing—review and editing (equal), conceptualization (equal), and methodology (equal). All authors have read and agreed to the published version of the manuscript.

Funding: This research received no external funding.

Data Availability Statement: Data are contained within the article.

Acknowledgments: The authors would like to thank the Deanship of Scientific Research at Shaqra University for supporting this work.

Conflicts of Interest: The authors declare no conflict of interest.

References

- Kumar, N.; Pandey, A.; Sharma, Y.C. A Review on Sustainable Mesoporous Activated Carbon as Adsorbent for Efficient Removal of Hazardous Dyes from Industrial Wastewater. *J. Water Process Eng.* **2023**, *54*, 104054. [\[CrossRef\]](#)
- Ahmadian, M.; Jaymand, M. Interpenetrating Polymer Network Hydrogels for Removal of Synthetic Dyes: A Comprehensive Review. *Coord. Chem. Rev.* **2023**, *486*, 215152. [\[CrossRef\]](#)
- Kausar, A.; Zohra, S.T.; Ijaz, S.; Iqbal, M.; Iqbal, J.; Bibi, I.; Nouren, S.; El Messaoudi, N.; Nazir, A. Cellulose-Based Materials and Their Adsorptive Removal Efficiency for Dyes: A Review. *Int. J. Biol. Macromol.* **2023**, *224*, 1337–1355. [\[CrossRef\]](#)
- Kaner, D.; Sarac, A. Removal of Dyes from Water Using Crosslinked Aminomethane Sulfonic Acid Based Resin. *Environ. Geochem. Health* **2010**, *32*, 321–325. [\[CrossRef\]](#)
- Bilal, M.; Khan, U.; Ihsanullah, I. MXenes: The Emerging Adsorbents for the Removal of Dyes from Water. *J. Mol. Liq.* **2023**, *385*, 122377. [\[CrossRef\]](#)
- Ma, J.; Zhang, M.; Ji, M.; Zhang, L.; Qin, Z.; Zhang, Y. Magnetic Graphene Oxide-Containing Chitosan-Sodium Alginate Hydrogel Beads for Highly Efficient and Sustainable Removal of Cationic Dyes. *Int. J. Biol. Macromol.* **2021**, *193*, 2221–2231. [\[CrossRef\]](#)

7. Ihaddaden, S.; Aberkane, D.; Boukerroui, A.; Robert, D. Removal of Methylene Blue (Basic Dye) by Coagulation-Flocculation with Biomaterials (Bentonite and *Opuntia Ficus Indica*). *J. Water Process Eng.* **2022**, *49*, 102952. [[CrossRef](#)]
8. Kono, H.; Kusumoto, R. Journal of Water Process Engineering Removal of Anionic Dyes in Aqueous Solution by Flocculation with Cellulose Ampholytes. *J. Water Process Eng.* **2015**, *7*, 83–93. [[CrossRef](#)]
9. Liu, Y.; Yan, A.; Ding, L.; Wei, J.; Liu, Y.; Niu, Y. Colloids and Surfaces A: Physicochemical and Engineering Aspects Simultaneous and Ultrafast Removal of Anionic and Cationic Dyes from Aqueous Solution by Zr-Based MOFs Hybridized by Attapulgite and Adsorption Performance Research. *Colloids Surf. A Physicochem. Eng. Asp.* **2024**, *680*, 132643. [[CrossRef](#)]
10. Semwal, N.; Mahar, D.; Chatti, M.; Dandapat, A.; Chandra, M. Heliyon “Adsorptive Removal of Congo Red Dye from Its Aqueous Solution by Ag-Cu-CeO₂ Nanocomposites: Adsorption Kinetics, Isotherms, and Thermodynamics”. *Heliyon* **2023**, *9*, e22027. [[CrossRef](#)]
11. Mahlangu, O.T.; Mamba, G.; Mamba, B.B. A Facile Synthesis Approach for GO-ZnO/PES Ultrafiltration Mixed Matrix Photocatalytic Membranes for Dye Removal in Water: Leveraging the Synergy between Photocatalysis and Membrane Filtration. *J. Environ. Chem. Eng.* **2023**, *11*, 110065. [[CrossRef](#)]
12. Subrahmanya, T.M.; Widakdo, J.; Mani, S.; Faye, H.; Hung, W.; Makari, H.K.; Nagar, J.K.; Hu, C.; Lai, J. An Eco-Friendly and Reusable Syringe Filter Membrane for the Efficient Removal of Dyes from Water via Low Pressure Filtration Assisted Self-Assembling of Graphene Oxide and SBA-15/PDA. *J. Clean. Prod.* **2022**, *349*, 131425. [[CrossRef](#)]
13. Duan, Y.; Zhao, J.; Qiu, X.; Deng, X.; Ren, X.; Ge, W.; Yuan, H. Coagulation Performance and Floc Properties for Synchronous Removal of Reactive Dye and Polyethylene Terephthalate Microplastics. *Process Saf. Environ. Prot.* **2022**, *165*, 66–76. [[CrossRef](#)]
14. Mcyotto, F.; Wei, Q.; Macharia, D.K.; Huang, M.; Shen, C.; Chow, C.W.K. Effect of dye structure on color removal efficiency by coagulation. *Chem. Eng. J.* **2021**, *405*, 126674. [[CrossRef](#)]
15. Liu, M.; Yin, W.; Zhao, T.; Yao, Q.; Fu, S.; Zhou, G. High-Efficient Removal of Organic Dyes from Model Wastewater Using Mg(OH)₂-MnO₂ Nanocomposite: Synergistic Effects of Adsorption, Precipitation, and Photodegradation. *Sep. Purif. Technol.* **2021**, *272*, 118901. [[CrossRef](#)]
16. Bayat, M.; Javanbakht, V.; Esmaili, J. Synthesis of zeolite/nickel ferrite/sodium alginate bionanocomposite via a co-precipitation technique for efficient removal of water-soluble methylene blue dye. *Int. J. Biol. Macromol.* **2018**, *116*, 607–619. [[CrossRef](#)]
17. Maria, S.; Guelli, D.A.; De Souza, U.; Angela, K.; Bonilla, S.; Augusto, A.; Souza, U. Removal of COD and Color from Hydrolyzed Textile Azo Dye by Combined Ozonation and Biological Treatment. *J. Hazard. Mater.* **2010**, *179*, 35–42. [[CrossRef](#)]
18. Wijannarong, S.; Aroonsrimorakot, S.; Thavipoke, P. Removal of Reactive Dyes from Textile Dyeing Industrial Effluent by Ozonation Process. *APCBEE Procedia* **2013**, *5*, 279–282. [[CrossRef](#)]
19. Yuan, J.; Chen, Z.; Yu, Q.; Zhu, W.; Li, S.; Han, L.; Lu, X.; Li, S.; Wu, Y.; Lv, Z.; et al. Enhanced Electrochemical Removal of Dye Wastewater by PbO₂ Anodes Using Halloysite Nanotubes with Different Surface Charge Properties. *J. Electroanal. Chem.* **2022**, *923*, 116816. [[CrossRef](#)]
20. Leng, Q.; Xu, S.; Wu, X.; Wang, S.; Jin, D.; Wang, P.; Wu, D.; Dong, F. Electrochemical Removal of Synthetic Methyl Orange Dyeing Wastewater by Reverse Electrodialysis Reactor: Experiment and Mineralizing Model. *Environ. Res.* **2022**, *214*, 114064. [[CrossRef](#)]
21. Khaled, J.M.; Alyahya, S.A.; Govindan, R.; Kanisha, C. Laccase Producing Bacteria Influenced the High Decolorization of Textile Azo Dyes with Advanced Study. *Environ. Res.* **2022**, *207*, 112211. [[CrossRef](#)]
22. Noman, E.; Talip, B.A.; Al-gheethi, A.; Mohamed, R.; Nagao, H. Materials Today: Proceedings Decolourisation of Dyes in Greywater by Mycoremediation and Mycosorption Process of Fungi from Peatland: Primary Study. *Mater. Today Proc.* **2020**, *31*, 23–30. [[CrossRef](#)]
23. Al-Wasidi, A.S.; Khairy, M.; Abdulkhair, B.Y.; Abdelrahman, E.A. Efficient Disposal of Basic Fuchsin Dye from Aqueous Media Using ZrO₂/MgMn₂O₄/Mg(Mg_{0.333}Mn_{1.333})O₄ as a Novel and Facilely Synthesized Nanocomposite. *Inorganics* **2023**, *11*, 363. [[CrossRef](#)]
24. Abdelrahman, E.A.; Algethami, F.K.; Alsalem, H.S.; Binkadem, M.S. Facile Synthesis and Characterization of Novel Nanostructures for the Efficient Disposal of Crystal Violet Dye from Aqueous Media. *Inorganics* **2023**, *11*, 339. [[CrossRef](#)]
25. Al-wasidi, A.S.; Abdelrahman, E.A. Simple Synthesis and Characterization of Cobalt Ferrite Nanoparticles for the Successful Adsorption of Indigo Carmine Dye from Aqueous Media. *Inorganics* **2023**, *11*, 453. [[CrossRef](#)]
26. Kirtimala, N.; Wareppam, B.; Herojit, L. Materials Today: Proceedings Effect of Sintering Temperature on the Magnetic Properties of ZnFe₂O₄ Composite with Cobaltic Oxide Synthesized by Chemical Co Precipitation Method. *Mater. Today Proc.* **2022**, *68*, 196–199. [[CrossRef](#)]
27. Chang, S.; Mei, S.; Yang, L.; Yang, L.; Lu, Z.; Shuang, W. Effect of Synthesis Conditions on the Structure and Properties of LiFeO₂/ZnFe₂O₄ Nanocomposites Prepared by a Sol-Gel Method. *Solid State Commun.* **2021**, *334–335*, 114379. [[CrossRef](#)]
28. Tiwari, N.; Kadam, S.; Ingole, R.; Kulkarni, S. Facile Hydrothermal Synthesis of ZnFe₂O₄ Nanostructures for High-Performance Supercapacitor Application. *Ceram. Int.* **2022**, *48*, 29478–29483. [[CrossRef](#)]
29. Srihari, S.; Panda, S.; Gandhi, S.; Reddy, S.; Panigrahi, T. Facile Hydrothermal Synthesis of Bio-Inspired ZnO/Fe₂O₃/ZnFe₂O₄ Heterostructure: Effect of Microwave Absorption Properties. *Surf. Interfaces* **2023**, *42*, 103490. [[CrossRef](#)]
30. Brandt, T.G.; Tuokkola, A.R.; Yu, M.; Laine, R.M. Liquid-Feed Flame Spray Pyrolysis Enabled Synthesis of Co- and Cr-Free, High-Entropy Spinel Oxides as Li-Ion Anodes. *Chem. Eng. J.* **2023**, *474*, 145495. [[CrossRef](#)]
31. Iljinas, A.; Brucas, R.; Stankus, V.; Dudonis, J. Synthesis of Fe₃O₄ Thin Films by Solid State Reactions. *Mater. Sci. Eng. C* **2005**, *25*, 590–594. [[CrossRef](#)]

32. He, X.; Guo, H.; Zhang, X.; Liao, T.; Zhu, Y.; Tang, H.; Li, T.; Song, J. ScienceDirect Facile Electrochemical Fabrication of Magnetic Fe₃O₄ for Electrocatalytic Synthesis of Ammonia Used for Hydrogen Storage Application. *Int. J. Hydrog. Energy* **2021**, *46*, 24128–24134. [[CrossRef](#)]
33. Ali, A.; Wijayantha, K.G.U.; Mazhar, M.; Mckee, V. ZnFe₂O₄ Thin Films from a Single Source Precursor by Aerosol Assisted Chemical Vapour Deposition. *Thin Solid Films* **2010**, *518*, 3664–3668. [[CrossRef](#)]
34. Gao, C.Y.; Baek, E.; You, C.Y.; Choi, H.J. Magnetic-Stimuli Rheological Response of Soft-Magnetic Manganese Ferrite Nanoparticle Suspension. *Colloid Polym. Sci.* **2021**, *4*, 865–872. [[CrossRef](#)]
35. Abdelrahman, E.A.; Abou El-Reash, Y.G.; Youssef, H.M.; Kotp, Y.H.; Hegazey, R.M. Utilization of Rice Husk and Waste Aluminum Cans for the Synthesis of Some Nanosized Zeolite, Zeolite/Zeolite, and Geopolymer/Zeolite Products for the Efficient Removal of Co(II), Cu(II), and Zn(II) Ions from Aqueous Media. *J. Hazard. Mater.* **2021**, *401*, 123813. [[CrossRef](#)]
36. Fayazi, M.; Afzali, D.; Taher, M.A.; Mostafavi, A.; Gupta, V.K. Removal of Safranin Dye from Aqueous Solution Using Magnetic Mesoporous Clay: Optimization Study. *J. Mol. Liq.* **2015**, *212*, 675–685. [[CrossRef](#)]
37. Mandal, B.; Kumar, S. Removal of Safranin T and Brilliant Cresyl Blue Dyes from Water by Carboxy Methyl Cellulose Incorporated Acrylic Hydrogels: Isotherms, Kinetics and Thermodynamic Study. *J. Taiwan Inst. Chem. Eng.* **2016**, *60*, 313–327. [[CrossRef](#)]
38. Abukhadra, M.R.; Mohamed, A.S. Adsorption Removal of Safranin Dye Contaminants from Water Using Various Types of Natural Zeolite. *Silicon* **2019**, *11*, 1635–1647. [[CrossRef](#)]
39. Shaban, M.; Abukhadra, M.R.; Shahien, M.G.; Khan, A.A.P. Upgraded Modified Forms of Bituminous Coal for the Removal of Safranin-T Dye from Aqueous Solution. *Environ. Sci. Pollut. Res.* **2017**, *24*, 18135–18151. [[CrossRef](#)]

Disclaimer/Publisher's Note: The statements, opinions and data contained in all publications are solely those of the individual author(s) and contributor(s) and not of MDPI and/or the editor(s). MDPI and/or the editor(s) disclaim responsibility for any injury to people or property resulting from any ideas, methods, instructions or products referred to in the content.